Investigations of grinding burn on a nitrided steel

B. Lavisse, Laurent Weiss, Ninel Kokanyan, André Lefebvre, Emerik Henrion, Olivier Sinot, Tidu Albert

Available online at www.sciencedirect.com

ScienceDirect

Procedia CIRP 108 (2022) 549–554

www.elsevier.com/locate/procedia

6th CIRP Conference on Surface Integrity

Investigations of grinding burn on a nitrided steel

B. Lavisse[a], L. Weiss[b], N. Kokanyan[c,d], A. Lefebvre[b], E. Henrion[b], O. Sinot[b], A. Tidu[b]

[a] *Arts et Métiers ParisTech, LAMPA, 2 bd du Ronceray, 49035, Angers, CEDEX, France*
[b] *Laboratoire d'Étude des Microstructures et de Mécaniques des Matériaux (LEM3), CNRS Université de Lorraine, F-57078 Metz cedex 03, France*
[c] *Chaire Photonique, LMOPS, CentraleSupélec, 2 rue E. Belin, 57070 Metz, France*
[d] *Université de Lorraine, LMOPS, 2 rue E. Belin, 57070 Metz, France*

* *Corresponding author:*
B. Lavisse [1]Arts et Métiers ParisTech, LAMPA, 2 bd du Ronceray, 49035, Angers, CEDEX, France. Tel +33241207343 e-mail bruno.lavisse@ensam.eu

Abstract

Grinding process may lead to the occurrence of grinding burn. When the temperature in the contact zone gets too high, it may lead to damage of the workpiece. The target of this study was to characterize changes occurring in the material after grinding burn on a nitrided steel. The microstructural changes after burn were quantified, by using residual stresses, Raman spectroscopy was also use to detect and characterize different oxides, appearing after grinding burn. The study highlights the possibilities of using this last non destructive method for detecting and quantifying grinding burn.

Keywords: Grinding burn, Microstructural Characterizations, Raman Spectroscopy

1. Introduction

When high surface quality standards are required on difficult-to-cut materials (hard and brittle for example), conventional machining as turning and milling may not be suitable. That is why abrasive machining and particularly grinding is widely used in mechanical component manufacturing industry. Actually, the surface quality obtained by grinding can be ten times better than that by turning or milling [1] and in many cases, grinding appears to be the more appropriate machining method to deal with difficult-to-cut materials [2]. However, this process requires a very high specific energy compared to other conventional machining processes. Indeed, the cutting speed in grinding is extremely high (between 30 and 100 m/s) and almost all the energy generated in the grinding zone is converted into heat, which is mainly dissipated into the surface of the workpiece [3]. This thermal energy comes from the plastic deformation strain appearing during the cutting and from the friction between workpiece and abrasive grains. Metallurgic damage is associated with high surface temperatures (it can reach 1000°C). High surface temperatures in grinding may result in visible surface damages of the workpiece. A blackish discoloration, cracks but also less noticeable microstructural changes on and below the surface (sometimes associated with a softening, or a re-hardening) may also occur [4]. Moreover, *Weiss et al* [5] observed in their work that the substrate is more likely to suffer from grinding burn than the chromium surface layer. Grinding burn includes one or more of the following surface defects: untempered martensite (UTM), overtempered martensite (OTM), oxidation and decarburization, superficial microcracks. Such phenomena, called grinding burn, reduces the life of the ground component and is very difficult to predict and to detect [6]. *Malkin et al* [7] worked on the critical maximum temperature principle and linked the thermal damaging process in grinding with the specific energy. *Bell et al* [8] also used this criterion to define a burn threshold in High Efficiency Deep Grinding. The authors worked on a modified approach for a burn threshold diagram, which takes into account the changes in the heat partition ratio by considering the Peclet number.

10.1016/j.procir.2022.03.086

In previous work, a critical temperature of 300°C has been defined for the grinding of a nitrided steel under oil lubrication [9]. Indeed, beyond this temperature, the cutting fluid boils and becomes inefficient in terms of cooling and lubricating. Then, an extreme increase of the temperature in the grinding zone can be seen. This thermal loading drastically deteriorates the mechanical properties of the machined material [10] and, from an industrial point of view, the occurrence of these defects often means the scrapping of the workpiece. The main goal of the present study is therefore to characterize changes, which occur in the material after a grinding, by using a conventional device such as X-Ray diffraction (XRD) to perform residual stress measurements, and by using Raman spectroscopy. Through this article, we would like to provide a better understanding of the grinding burn, especially of the thermomechanical damages located at the outer surface of the materials (where blacklish grooves occur) and of the presence of oxides in these areas. We would also like to demonstrate that Raman spectroscopy might be used as a consistent non-destructive monitor of the occurrence of burn.

2. Material and methods

2.1. Grinding machines

All tests have been done on surface grinding machines: a deep cut grinder HEDG DANOBAT RT1200CF and a surface grinder HAUNI-BLOHM Planomat 412.

2.2. Material properties

The studied material is a nitrided 32CrMoV12-9 steel made by tempering in nitrogen atmosphere at 600°C for 6 hours. Nitriding is of big interest for mechanical application. It guarantees a greater wear resistance by improving the surface hardness and enables a greater corrosion and seizure resistance. Moreover, this treatment generates compressive residual stresses, which improve the material fatigue life as explained in the work of *Barallier* [11] but also in the study of *Ghiglione et al* [12].

2.3. Material characterization

The ground surfaces were investigated by residual stresses using the $\sin^2\psi$ were measured on a D5000 goniometer from Brucker composed of a chromium X-ray source, a goniometric cradle and a linear position-sensitive detector. Finally, a confocal Raman microscope LabRAM HR Evolution (*Horiba*) was used which is equipped with a linear piezo-driven stage with a 532 nm wavelength laser. The laser light was focused through a x100 objective (*Olympus*). The mentioned Raman system leads to a spectral resolution of 1 cm^{-1}.

2.4. Temperature estimation

As explained, a too high elevation of temperature in the grinding zone may damage the workpiece. That is why an estimate of the temperature rise in this area is of great interest in view to explain the changes that eventually affect the workpiece microstructure.
Considering unidimensional heat exchanges between wheel and workpiece during grinding, a good approximation of the maximum background temperature rise in the contact area may be done with Eq.1 [13].

$$T_{maxi} = \beta \frac{R_w P_t}{b\sqrt{l_c}\sqrt{(\lambda\rho C)_w v_w}} \quad \text{Eq.1}$$

with b the wheel width, l_c the geometric contact length, $\sqrt{(\lambda\rho C)_w}$ the workpiece material thermal effusivity, β a constant depending on the heat flux shape and R_w the heat partition ratio (ratio of the heat fluw absorbed by the workpiece over the cutting power), P_t the cutting power and v_w the workpiece speed. β and R_w were defined thanks to previous works [14]. β is equal to 1.16, and R_w is equal to 0.85 for dry cutting and 0.43 for wet cutting.
In the following sections, the value T_{maxi} detailed in Eq 1 will be used to estimate the maximum temperature in the contact zone.

3. Grinding burn detections

In this section a grinding set up was defined on small samples. Then grinding burn were chemically characterized in terms of oxides after dry and wet conditions. Moreover a study of residual stresses after grinding pass under lubrication, which is more representative of industrial conditions, was also carried out.
Therefore, two types of tests were made: a first one under dry cutting conditions and a second one under wet cutting conditions.

3.1. Dry tests

In this section, the constant grinding parameters are the workpiece speed (v_w=0.033 m/s) and the wheel speed (v_s=32 m/s). Table 1 gives the grinding parameters. It is crucial to know precisely the real depth of cut on each grinding pass, to be sure that a change in the measured forces may be attributed to a varying depth of cut and not to a change in the contact between the wheel and the workpiece.
Because of machine uncertainty and possible workpiece expansion, the uncertainty of the nominal depth of cut (depth of cut set on the grinding machine) is about ± 3 µm. Therefore, for each pass, the real depth of cut is measured with a LVDT sensor (Linear Variable Differential Transformer, AX/2.5/S, measuring range ± 2.5 mm). This operation is detailed in a previous work [9]. In order to limit the effect of wear, the wheel was dressed before every passes.

Table 1. Grinding and dressing parameters

Wheel speed v_s	32 m/s		
Workpiece speed v_w	0.033 m/s		
Nominal depth of cut a_e	5-30-40 µm		
Aluminium oxide wheel	grit mesh size: 80	Average grain diameter: 165 µm	
Single point Dressing	$u_d = 2$	v_s = 32 m/s	a_{ed} = 10 µm

3.2. Tests under lubrication

These tests were made under neat oil lubrication (44 L/min flowrate) and a different strategy to reach the grinding burn has been proposed. It has been shown that the heat partition ratio (R_w) is extremely weaker under neat oil lubrication compared to dry passes (0.43 and 0.85, respectively). Therefore, to obtain the same temperature for a wet cutting pass as a dry one, a cutting power about two time greater is needed. Then it involves to extremely increase the depth of cut which is not material saver.

To avoid an overconsumption of material, the nominal depth of cut has been fixed to 20µm and the dressing conditions have been changed to vary the grinding conditions. It is well known that an increase in the overlap ratio exhibits a low effective surface roughness with a large number of grits. Because of increased friction and the large number of cutting edges, the particular forces add up to a larger total grinding forces. *Kadivar et al* [15] illustrate these phenomena in their works.

In the present paper, these tests were made on 20 mm cubes of 32CrMoV12-9 nitrided steel and three grinding conditions were aplied: “gentle”, “medium” and “severe”. The first sample was grinded with soft grinding conditions. In that last case the nominal depth of cut is 20 µm and the dressing overlap ratio is only 2. Therefore, the grinding wheel was in a very sharp state and generated low cutting forces. Actual knowledge ensured to obtain a safe material (without any burn) with those grinding conditions [9]. The second sample was machined with medium grinding conditions since a 6 dressing overlap ratio was used. At last, the third sample was machined with severe grinding conditions after a 7.5 dressing overlap ratio. Once again, the use of previous works guarantees the occurrence of grinding burn on the material for these conditions.

Table 2 summarizes grinding conditions for the three samples.

Table 2. Grinding and dressing parameters

Grinding wheel speed v_s (m/s)	Grinding wheel diameter (mm)	Workpiece speed v_w (mm/min)	Nominal depth of cut a_e (µm)	Dressing overlap ratio u_d
32	336	2000	20	Variable : 2 ; 6 ; 7.5

It was also ensured that the depth of cut was not varying along the grinding pass between the three samples by using the same LVDT sensor as for the dry tests.

3.3. Occurrence of grinding burn related to the predicted temperature

The Figure 1 presents the surface appearance for different grinding conditions. The grinding burn was obtained for an increase of the depth of cut in dry cutting and by increasing the overlap ratio in wet conditions. It may be observed that severe grinding conditions (sample C in Fig.1b) led, as predicted, to the occurrence of burning marks on the material. At the opposite, the two others (A and B) present no visible damages. This material damage is characterized by its blackish discoloration, which suggest once again as the thin layer displayed on the Figure 1, the presence of metallic oxides. The nature of these oxides were revealed by Raman spectroscopy.

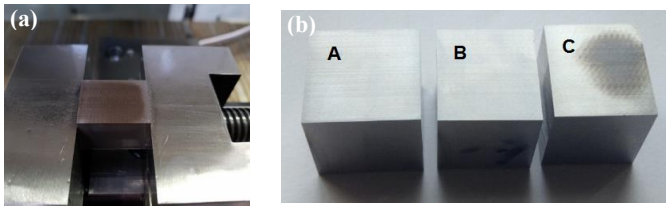

Fig. 1. a) Dry grinding burn b) Grinding material for three conditions under lubrication "gentle", "medium" and "severe"

The Table 3 details the grinding condition and maximum temperature in the contact zone for all conditions. These temperatures were estimated thanks to eq 1. We can notice that for every burned surfaces, the maximum temperature was in a range of 700°C to 830°C, that is in the order of the austenitization temperature.

Table 3. Grinding and dressing conditions with the maximum temperature in the contact zone associated

	Dry Safe	**Dry Burned 1**	**Dry Burned 2**	**Wet Gentle A**	**Wet Medium B**	**Wet burned C**
v_s (m/s)	32	32	32	32	32	32
v_w (m/min)	2	2	2	2	2	2
a_e real (µm)	6	42	50	17	18	26
u_d	4	4	4	2	6	7.5
Température (°C)	300°C	710	833	152	190	770

3.4. Oxides detection by Raman spectroscopy

Surface oxidation of a high-value component is unacceptable due to the risk of sub-surface metallurgical damage and the development of residual tensile stresses. Raman spectroscopy is rarely used to analyze machined surfaces (either for classical cutting processes or grinding). Yet, it is a promising technique since it characterizes the changes that occur inside the

workpiece in an effortless way. By characterizing the external surface of the samples in a non-destructive way, the use of this technic enables the changes in the chemical structure of the workpiece (particularly the iron oxides in the present case) to be detected [16]. As those microstructural changes occur after grinding burn, we can suppose that Raman spectroscopy could be a way to detect and also quantify a grinding burn. The first burnt sample to be observed corresponds to the dry burn 1 in Table 3. A Raman mapping was performed on the surface of this sample (9.5 x 5.5 mm). The step size between each mapping point was fixed to be 500 μm. Figure 2 illustrates Raman spectra recorded at different areas of the sample. Obtained spectra could be merged according to different burnt areas of the surface. It can be mentioned that no oxide has been detected in the spectrum (in black) corresponding to the non-burnt area. Moving to more burnt areas (blue spectrum), one can notice the appearance of iron oxide on the surface identified in Raman spectra with maghemite and hematite vibrational modes [17]. In relatively more burnt regions, Raman spectra (in orange) show the increase of intensities of hematite comparing to the previous case. In addition, half of the linewidths of corresponding Raman modes are lower, which means the crystallization of hematite oxides

Finally, spectra corresponding to the most burnt regions (in brown) show, on one hand, the extinction of maghemite modes and a noticeable decrease of hematite modes, and, on the other hand, the appearance of magnetite. Figure 3 illustrates the ratio of magnetite/maghemite on the surface of the sample. One can notice three areas with different burning rates. On the right side of the surface, where there is only the metal, the ratio is near 0, and on the left side, which corresponds to the most burning rate the ratio is the highest, as the magnetite is dominant in this area. Same measurements were carried out for the Dry Burned 2 sample and similar results were obtained.

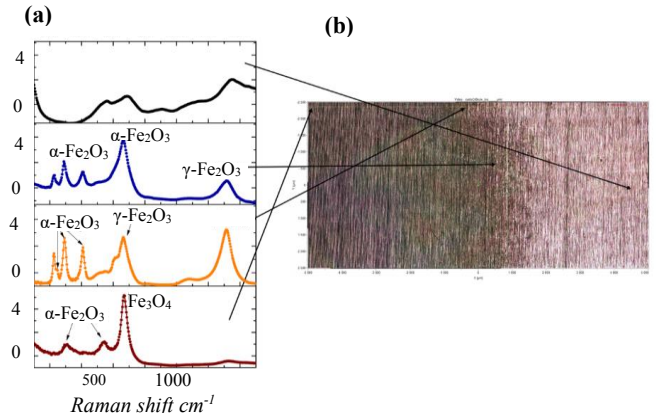

Fig. 2 Sample Dry Burned 1: a) Raman spectra associated to different areas b) micrograph of the surface

Other Raman spectra were also carried out on samples ground under wet conditions. The safe and burnt sample were analyzed (Wet A and Wet C in the Table 3.) One can be noticed the presence of the same oxides as under dry conditions: hematite α-Fe_2O_3 and magnetite Fe_3O_4 on the burnt sample (Figure 4.) However, no oxide were detected on the Wet A sample.

It reveals, that the grinding burn is quite similar under dry or wet conditions. Indeed, the occurrence of grinding burn totally cancels the benefits of fluid in term of cooling and friction [9].

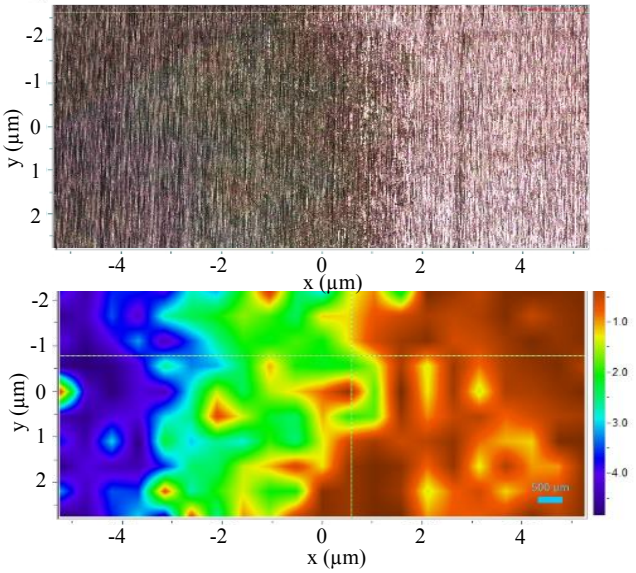

Fig. 3 Mapping of the ratio of integrated intensities of Raman modes at 661 cm^{-1} (maghemite) and 1310 cm^{-1} (magnetite)

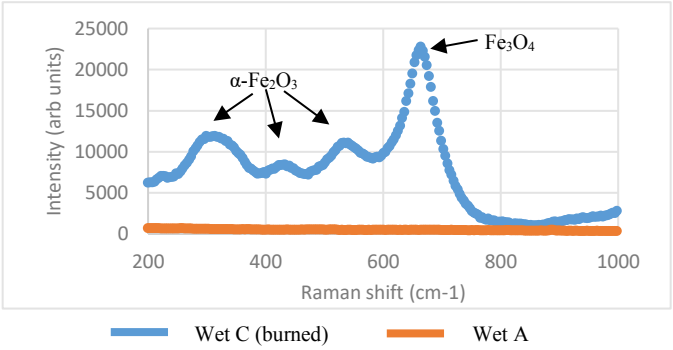

Fig. 4 Raman spectra associated to the wet burn sample (C) and the wet dry sample (A)

The different oxides found in this study are the same than which were found in other type of high-energy cutting processes like laser-water jet cutting [18] but their presence has not been explained accurately through temperatures analysis.

The presence of the different iron oxides as a function of the visual intensity of the burn (Figure 2-3) makes it possible to fully define a theory of the appearance of these burn spots. Initially, at room temperature, according to the phase diagram in the Figure 5 [19], the thin invisible layer of oxide is composed of magnetite Fe_3O_4 and hematite α-Fe_2O_3. As the sample warms up, a visible oxide layer is observed and corresponds to the appearance of brown γ-Fe_2O_3 maghemite (an intermediate compound between magnetite and hematite). The results of [17] showed that the formation of this oxide is explained by the destabilization of the magnetite from around 200°C then, at around 400°C, maghemite transforms into red hematite. When the temperature still increases (average temperature of high burn samples may be close to 900° C but the local temperature much higher), the remaining maghemite and hematite turn into magnetite according to the phase diagram. Magnetite has a natural black color, which is why heavily burned areas appear darker and darker, in accordance

with the magnetite ratio. However, we can notice that no chromium or vanadium oxides have been detected.

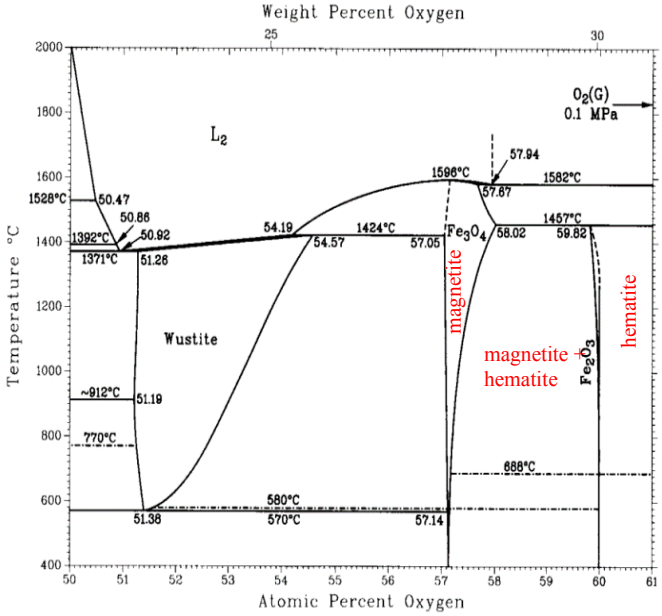

Fig.5: Iron-Oxygen phase diagram from [19]

In a study of burn behaviors of grinding rail, *Lin et al* [20] described a correlation between the occurrence of oxides and using XRD and find an increase in the presence of Magnetite when the grinding burn is increasing. That is in accordance with our results.the grinding burn severity. They observed these oxides by using XRD and find an increase in the presence of Magnetite when the grinding burn is increasing. That is in accordance with our results.

3.5. Grinding induced residual stresses

Surface residual stresses are of great importance [21] for the durability of ground mechanical pieces (gear, landing gear, sliding cylinder, valve…). *Yu et al* [22] also showed that stretch grinding can, reduce the residual tensile stress in the surface layer of the workpiece or even convert the residual tensile stress into residual compressive stress. The origins of residual stresses in ground workpiece have been investigated for many decades and it was found that thermal expansion and contraction due to the thermal loading was the most significant factor in the generation of tensile residual stresses as explain in the work of [23] and that of [24]. That is why, this is crucial to get a strong knowledge of the stresses evolution depending on cutting parameters. Moreover, the lack of visible burning discolorations is not a sufficient condition to fully ensure that any changes in material microstructure had occurred in sub-surface. The oxidation can be polished off after grinding and the surface appearance restored. Then, XRD (surface) residual stresses measurement was done on the 3 wet samples to identify the influence of the severity of the grinding pass on the residual stresses state of the ground material under lubrication.

Residual stresses are determined with the ferrite family of planes {211}. Following mechanical properties was used: 210 GPa for the Young Modulus and 0.28 for the Poisson's ratio. Results are presented on the Figure 6.

For gentle and medium grinding conditions (without any visible burning marks), compressive stresses are obtained in principal directions (σ_{11} grinding direction et σ_{22} perpendicularly to the grinding direction). The occurrence of surface compressive residual stresses after safe grinding passes is a well-known phenomenon [25].

Then, we can observe that severe grinding pass provoke an important increase in the residual stresses until achieving tensile stresses for the σ_{22} direction.

These results are in accordance *Cortial et al* [26] who showed that an increase in the severity of grinding pass (in their case an increase in depth of cut) is followed by a decrease in the residual compressive stresses on the ground surface. At last, as in their study, we found stronger stresses perpendicularly to the direction of the workpiece speed, than to the parallel direction.

Many papers have shown that there does exist the most direct relationship between workpiece burn and grinding temperature. *Chen et al* [23] defined the transitional temperature for tensile residual stress in steel, which is strongly depending on the material properties. It is also interesting to compare changes in residual stresses with the maximal temperature evolution in the grinding zone. This temperature is a reliable indicator of the occurrence of a change in terms of microstructural state (austenitization or retemper temperature overtake for example). Therefore, by using the temperature calculation model defined previously and based on the model of *Guo* [27], coming from *Jaeger* [28] and described in the Eq 1, but also by considering the thermal characteristics of the material and finally the cutting forces measurement, the temperature in the contact zone has been calculated for all the grinded tests. For tests which did not show any burning discoloration, a 0.43 heat partition ratio was chosen [14] whereas for the other a 0.85 heat partition ratio was chosen. Actually, it has been shown that the occurrence of grinding burn totally cancels the benefits of fluid in term of cooling and friction [9]. Therefore, these tests can be seen as similar to those obtained after dry grinding.

In the Figure 6 residual stresses were also associated for each test with the corresponding maximum predicted temperature in the contact zone. For the "gentle" and "medium" grinding conditions samples, the maximum temperatures in the contact zone included are 150°C and 200°C. These temperatures are very far from the tempering temperature of the bulk material (600°C) and have no effect on the level of residual stresses of the grinded material. For safe grinded samples the level of σ_{11} compressive stresses is about 450 MPa and 550 MPa for σ_{22}. However, when the grinding burn occurs, the absence of fluid efficiency and the sudden burst of cutting forces are leading to very a high temperatures in the contact zone (about 800°C for the sample C). It can be noticed that this temperature (close to the austenitization temperature) creates tensile residual stresses in the cutting direction. These types of stresses have excessive harmful effects because they can lead to cracks occurrence perpendicularly to the grinding direction.

At last, σ_{22} residual stresses are increasing during the occurrence of grinding burn but in a less significant way than the σ_{11} stresses.

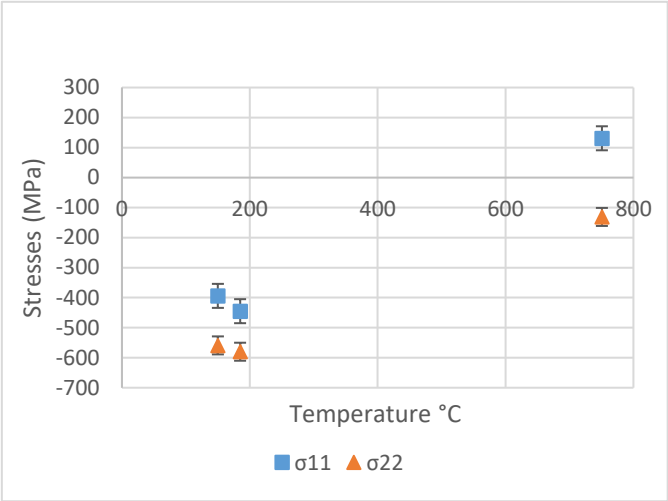

Fig. 6: Residual surface stresses parallel σ11 and perpendicularly σ22 to the grinding direction vs the maximum temperature in the contact zone for three cutting conditions (gentle, medium and severe)

4. Conclusion

In this study, the thermal damage of the material due to grinding burn was characterized by a decrease in the residual compressive stresses (in absolute terms) until becoming tensile stresses when the grinding temperature is close to 800°C. The residual stress measurements applied to the detection of grinding burn have the advantages of high accuracy and comprehensive analysis while being non-destructive. Indeed, the severity of the burn can easily be quantified by the level of tensile. However this method also suffer from limitations such as high cost and complicated operation which not be perfectly suitable for industrial applications.

The results coming from the NDT method, Raman Spectroscopy, showed that the oxide detection on a grinded sample enable surface grinding burn to be localized and characterized with an important accuracy and efficiency. As XRD measurements Raman Spectroscopy has demonstrated its ability to quantify grinding burn. When these burn occurs, oxides appear, and may be detected easily and quickly by Raman spectroscopy whatever the use of lubrication or not. Moreover, this device may quantify the intensity of the burn but also precisely localize the damages. The determination of the nature of the oxides may also be a reliable way to estimate the grinding temperature in the contact zone just after the pass. Raman mapping appears to be a very promising ways to characterize and detect grinding burn. It could be therefore very interesting to use Raman spectroscopy for industrial application (NDT, quickness of measurements), and it deserves to be further analyzed in future studies.

References

[1] A. Beranoagirre and L. N. Lopez de Lacalle, "Grinding of Gamma TiAl Intermetallic Alloys," *The Manufacturing Engineering Society International Conference, MESIC 2013,* vol. 63, pp. 489-498, 2013.

[2] B. S. Linke and D. A. Dornfeld, "Application of axiomatic design principles to identify more sustainable strategies," *Journal of Manufacturing Systems,* vol. 31, pp. 412-419, 2012.

[3] E. Brinksmeier, C. Heinzel and M. Wittmann, "Friction, Cooling and Lubrication in Grinding," *CIRP Annals - Manufacturing Technology,* vol. 48, pp. 581-598, 1999.

[4] D. A. Lucca, E. Brinksmeier and G. Goch, "Progress in Assessing Surface and Subsurface Integrity," *Annals of the CIRP,* vol. 47, pp. 669-693, 1998.

[5] B. Weiss, A. Lefebvre, O. Sinot, M. Marquer and A. Tidu, "Effect of grinding on the sub-surface and surface of electrodeposited chromium and steel substrate," *Surface and Coatings Technology,* vol. 272, pp. 165-175, 2015.

[6] I. S. Jawahir, E. Brinksmeier, R. M'Saoudi, D. K. Aspinwall, J. C. Outeiro, D. Meyer, D. Umbrello and A. D. Jayal, "Surface integrity in material removal processes: Recent advances," *CIRP Annals - Manufacturing Technology,* vol. 60, pp. 603-626, 2011.

[7] S. Malkin and C. Guo, "Thermal Analysis of Grinding," *CIRP Annals - Manufacturing Technology,* vol. 56, pp. 760-782, 2007.

[8] A. Bell, T. Jin and D. J. Stephenson, "Burn Threshold Prediction for High Efficiency Deep Grinding," *International Journal of Machine Tools and Manufacture,* vol. 51, pp. 433-438, 2013.

[9] B. Lavisse, A. Lefebvre, A. A. Torrance, O. Sinot, E. Henrion, S. Lemarié and A. Tidu, "The effects of the flow rate and speed of lubricoolant jets on heat transfer in the contact zone when grinding a nitrided steel," *Journal of Manufacturing Processes,* vol. 35, pp. 233-243, 2018.

[10] M. Sinha, D. Setti, S. Ghosh and P. Rao, "An investigation on surface burn during grinding of Inconel 718," *Journal of Manufacturing Processes,* vol. 21, pp. 124-133, 2016.

[11] L. Barrallier and S. Jégou, "Traitement de nitruration et durabilité des pièces mécaniques," *HAL,* pp. 1-10, 2015.

[12] D. Ghiglione, C. Leroux and C. Tournier, "Nitruration, nitrocarburation et dérivés," *Techniques de l'ingénieur,* pp. 1-49, 1996.

[13] W. B. Rowe, S. C. Black, B. Mills, H. S. Qi and M. N. Morgan, "Experimental Investigation of Heat Transfer in Grinding," *CIRP Annals,* vol. 44, pp. 329-332, 1995.

[14] B. Lavisse, A. Lefebvre, O. Sinot, E. Henrion, S. Lemarié and A. Tidu, "Grinding heat flux distribution by an inverse heat transfer," *International Journal of Advanced Manufacturing Technology,* vol. 92, pp. 2867-2880, 2017.

[15] M. Kadivar, B. Azarhoushang, S. Shamray and P. Krajnik, "The effect of dressing parameters on micro-grinding of titanium alloy," *Precision Engineering,* vol. 51, pp. 176-185, 2017.

[16] R. Marcelo Do Nascimento, A. Baldit, N. Kokanyan, L. K. Tappert, P. Lipinski, A. C. Hernandes and R. Rahouadj, "Mechanical-Chemical Coupling in Temporomandibular Joint Disc," *Materialia,* vol. 9, 2020.

[17] D. L. De Faria, S. V. Silva and M. T. Oliveira, "Raman Microspectroscopy of Some Iron Oxides and Oxyhydroxides," *Journal of Raman Spectroscopy,* vol. 28, pp. 873-878, 1997.

[18] L. Weiss, M. Ailerie, A. A. Tazibt and A. Tidu, "Surface oxidation and phase transformation of the stainless steel by hybrid laser-waterjet impact," *Materials Research Express,* vol. 1, 2014.

[19] H. A. Wriedt, "The Fe-O (Iron-Oxygen) System," *Journal of Phase Equilibria,* vol. 12, pp. 170-200, 1991.

[20] B. Lin, K. Zhou, J. Guo, Q. Y. Liu and W. J. Wang, "Influence of grinding parameters on surface temperature and burn behaviors of grinding rail," *Tribology International,* vol. 122, pp. 151-162, 2018.

[21] S. O. Hel-Helieby and G. W. Rowe, "A quantitative comparison between residual stresses and fatigue properties of surface-ground bearing steel," *Wear,* vol. 58, pp. 155-172, 1980.

[22] X. X. Yu and W. S. Lau, "A finite-element analysis of residual stress in stretch grinding," *Journal of Materials Processing Technology,* vol. 94, pp. 13-22, 1999.

[23] W. R. D. M. X. Chen, "Analysis of the transitional temperature for tensile residual stress in grinding," *Journal of Materials Processing Technology,* vol. 107, pp. 216-221, 2000.

[24] W. Ding, L. Zhang, Z. Li, Y. Zhu, H. Su and J. Xu, "Review on grinding-induced residual stresses in metallic materials," *International Jounal of advanced Manufacturing Technology,* vol. 88, pp. 2939-2968, 2017.

[25] J. Zang, G. C. Wang, H. J. Pei and G. C. Wang, "Effects of grinding parameters on residual stress of 42CrMo steel surface layer in Grind-hardening," *Advances in Engineering Research,* vol. 134, 2018.

[26] F. Cortial, C. Le Gall and J. Guibreteau, "Rectification de denture de reducteurs nitrurées à l'aide de meules en CBN," *Matériaux & Techniques,* Vols. 7-8, pp. 39-45, 1997.

[27] C. Guo and S. Malkin, "Inverse Heat Transfer Analysis of Grinding Part 1 Methods," *Journal Engineering of Industry,* vol. 118, pp. 137-142, 1996.

[28] J. C. Jaeger, "Moving sources of heat and the temperature at sliding contacts," *Proc. R. Soc. NSW,* vol. 76, pp. 203-224, 1942.